Hybrid fluid/kinetic modeling of Pluto's escaping atmosphere ☆

Justin Erwin[a], OJ Tucker[b], Robert E Johnson[a,c]

[a]*Department of Engineering Physics, University of Virginia, 166 Engineers Way, P.O. Box 400745, Chalottesville, VA 22904*
[b]*Department of Atmospheric, Oceanic and Space Science, University of Michigan, Ann Arbor, MI 48109*
[c]*Department of Physics, New York University, New York, New York, 10012*

Abstract

Predicting the rate of escape and thermal structure of Pluto's upper atmosphere in preparation for the New Horizons Spacecraft encounter in 2015 is important for planning and interpreting the expected measurements. Having a moderate Jeans parameter Pluto's atmosphere does not fit the classic definition of Jeans escape for light species escaping from the terrestrial planets, nor does it fit the hydrodynamic outflow from comets and certain exoplanets. It has been proposed for some time that Pluto lies in the region of slow-hydrodynamic escape. Using a hybrid fluid/molecular-kinetic model, we previously demonstrated the typical implementation of this model fails to correctly describe the appropriate temperature structure for the upper atmosphere for solar minimum conditions. Here we used a time-dependent solver to allow us to extend those simulations to higher heating rates and we examined fluid models in which Jeans-like escape expressions are used for the upper boundary conditions. We compare these to our hybrid simulations of the atmosphere under heating conditions roughly representative of solar minimum and medium conditions as these bracket conditions expected during the New Horizon encounter. Although we find escape rates comparable to those previously estimated by the slow-hydrodynamic escape model, and roughly consistent with energy limited escape, our model produces a much more extended atmosphere with higher temperatures roughly consistent with recent observations of CO. Such an extended atmosphere will be affected by Charon and will affect Pluto's interaction with the solar wind at the New Horizon encounter. Since we showed earlier that such models can be scaled, these results have implications for modeling exoplanet atmospheres for which the energy limited escape approximation is often used.

Keywords: Pluto, Pluto, atmosphere, Aeronomy, Atmospheres, structure, Atmosphere, dynamics

1. Introduction

Recent spacecraft exploration of the planets and moons in our solar system and the rapid increase in the discovery of exoplanets has increased interest in atmospheric escape from planetary bodies. The Cassini spacecraft is currently improving our understanding of atmospheric escape from Titan, while in 2015 the New Horizons (NH) spacecraft will flyby Pluto performing occultation observations of its and Charon's atmosphere, and the Maven mission will orbit Mars studying the composition of its escaping atmosphere. Furthermore, newly discovered exoplanets with radii ranging from just a few times that of Earth to of the order of Jupiter have been discovered, and their atmosphere's also modeled (Lammer et al., 2009; Murray-Clay et al., 2009; Yelle, 2004). Here we

carry out simulations of Pluto's upper atmosphere that include atmospheric loss by thermal escape that can be tested against data to be obtained during the NH encounter. By accurately describing the present loss rates, one can in principle learn about the evolution of Pluto's atmosphere. In addition, doing this accurately for a planet for which we will have in situ spacecraft data can, by scaling, guide our ability to model exoplanet atmospheres for which there will only be remote sensing data.

The previous models of atmospheric escape for Pluto used the concept of hydrodynamic escape by adapting the *critical solution* in Parker (1964). Parker described the expanding stellar corona and stellar wind assuming the temperature and pressure go to zero at infinity, and showed that for this to happen the bulk velocity must increase past the isothermal speed of sound at a critical point that is dependent on the temperature and gravity.

This model was subsequently adapted for planetary atmospheres to include heating by solar radiation (McNutt,

1989; Hunten and Watson, 1982) and was applied to Pluto (Krasnopolsky, 1999; Strobel, 2008) and Titan (Strobel, 2009). It is often referred to as the slow-hydrodynamic escape (SHE) model. The model required solving the fluid equations out to very large distances from the planet to enforce the necessary boundary conditions. However, it is known that at some finite distance the equations of fluid dynamics fail to describe the flow of mass, momentum and energy in an atmosphere (Volkov et al., 2011; Johnson, 2010). The region of validity of the fluid equation is often classified using the Knudsen number, $Kn = \ell/H$, the ratio of the mean free path of the molecules, $\ell = (\sqrt{2}\sigma n)^{-1}$, to the density scale height, $H = \frac{k_b T}{GMm/r^2}$, of the atmosphere. The fluid equations apply well where $Kn \ll 1$ so that many collisions occur over relevant length scales keeping the gas in thermal equilibrium.

The concept of energy limited escape, which we will also examine here, is heavily used in modeling escape from early terrestrial planet atmospheres (Tian et al., 2009) and the growing body data on exoplanet atmospheres (Lammer et al., 2009; Valencia et al., 2010). For an atmosphere heated by EUV radiation, assuming that kinetic and thermal energy terms are small compared to gravity, and the thermal conduction is inefficient, the molecular loss rate is often approximated as

$$\phi_L \approx \frac{Q}{U(r_p)} \tag{1}$$

Here Q is the EUV energy supplied in the upper atmosphere, and $U(r) = GMm/r$ is the gravitational energy. Without doing a detailed heating model one can use $Q = \pi r_{EUV}^2 \eta F_{EUV}$, where r_{EUV} is the mean radius at which the radiation is absorbed and η and F_{EUV} are the heating efficiency and solar energy flux respectively. This depends critically on r_{EUV} which is sometimes assumed to be close to the visual radius so that r_p can be used. The radius used to evaluate the gravitational potential is uncertain, with r_p being a good option for terrestrial planets.

The alternative to organized outflow is evaporative escape, by which the atmosphere loses gas on a molecule-by-molecule basis driven by conductive heat flow from below. The standard analytic model was originally developed in Jeans (1925) and is referred to as Jeans escape. The escape rates are found to depend predominately on the Jeans parameter $\lambda = GMm/rk_b T$, the ratio of gravitational to thermal energy of the molecules. For large Jeans parameter the escape rate is obtained by integrating the velocity distribution over the portion of molecules that are upward moving with speed in excess of the escape

velocity. Assuming a Maxwell-Boltzmann velocity distribution the molecular escape rate ϕ and energy escape rate ϕ_E from a altitude r are given by

$$\langle \phi \rangle_J = \frac{1}{4} n \bar{v} \cdot (1 + \lambda) \exp(-\lambda) \cdot 4\pi r^2 \tag{2}$$

$$\langle \phi_E \rangle_J = \langle \phi \rangle_J \cdot k_b T \left(\frac{C_p}{k_b} - \frac{3}{2} + \frac{1}{1 + \lambda} \right) \tag{3}$$

Here $\bar{v} = \sqrt{8 k_b T/m\pi}$ is the med molecular speed. To be consistent with the fluid equations, we also consider expressions which apply a drifting Maxwell-Boltzmann to include the bulk velocity u in the velocity distribution (Yelle, 2004; Tian et al., 2009; Volkov et al., 2011). Typically these equations are applied at a level called the exobase where $Kn \approx 1$, as there are few collisions above this level to inhibit a molecule from escaping.

Accurate calculations of thermal escape can be obtained, in principle, by solving the Boltzmann's equation or, more often, by using the Direct-Simulation Monte-Carlo (DSMC) model as in Tucker and Johnson (2009) and Volkov et al. (2011). In this method, representative particles are used along with a model of molecular collisions to calculate the temperature, density and other macroscopic values from the velocity distribution in both the dense and rarified regions. In this respect, DSMC can model the exospheres with better accuracy than hydrodynamics model, but can only model the lower, denser regions of the atmosphere at great computational cost. Using the DMSC method Volkov et al. (2011) demonstrated earlier that for a monatomic or diatomic gas in the absence of heating above some lower boundary for $\lambda \gtrsim 3$ the escape is Jeans-like at the exobase (i.e. $\phi/\langle \phi \rangle_J \approx 1.5$ for the range of Jeans parameters studied). For our model of Pluto, the lower boundary of the simulated domain has $\lambda = 22.8$, and the exobase values exceed 4. Using the above results as guidance, we model the principal component in Pluto's atmosphere to obtain a description relevant to the NH encounter to test energy-limited escape, and to better understand the transition from Jeans to hydrodynamic escape.

2. Model Description

The steady state equations of mass, momentum, and energy have been used to study hydrodynamic escape. They can be solved to give the radial dependence of number density n, outward bulk velocity u, and temperature T in the region in which the atmosphere is collisional. However, as we have shown (Tucker et al., 2012; Volkov et al., 2011) they cannot be used by themselves to determine the

escape rate unless the Jeans parameter is very small in which case the solutions are somewhat insensitive to the boundary condition at infinity. The equations, neglecting viscosity can be written as

$$4\pi r^2 nu = \phi \tag{4}$$

$$nm\frac{\partial}{\partial r}\left(\tfrac{1}{2}u^2\right) + \frac{\partial p}{\partial r} = -n\frac{GMm}{r^2} \tag{5}$$

$$\frac{\partial}{\partial r}\left(\phi\left(C_pT + \tfrac{1}{2}mu^2 - \frac{GMm}{r}\right) - 4\pi r^2\kappa(T)\frac{\partial T}{\partial r}\right)$$
$$= 4\pi r^2 q(r) \tag{6}$$

Here ϕ is the molecular escape rate through the one dimensional atmosphere, p is the pressure (related via the equation of state, $p = nk_bT$), m is the mass of N_2 molecule, G is Newton's gravitational constant, M is the mass of Pluto, k_b is Boltzmann's constant, $\kappa(T)$ is the conductivity, $C_p = \frac{7}{2}k_b$ is the specific heat at constant pressure, and $q(r)$ is the net heating/cooling rate per unit volume. In Eq. (6), the first term on the left side is work done by adiabatic expansion and the second is the work done by conduction.

For the conductivity, we use the power law $\kappa(T) = \kappa_0 T^s$ to approximate the temperature dependence. Some authors use an empirical fit for the conductivity, e.g., Hunten and Watson (1982) used $s = 1.12$. While McNutt (1989) used $s = 1$ since it simplifies the analytic solutions to Eq. (6). In this paper we use $\kappa_0 = 9.37 \times 10^{-5}$ J/m K and $s = 1$ to compare with Strobel (2008) and because this is consistent with the variable-hard-sphere model for nitrogen molecule collisions, including translation/rotational coupling, used in DSMC models of the exosphere (Tucker et al., 2012; Volkov et al., 2011).

The radiative heating and cooling model is adapted from Strobel (2008), using the same fixed mixing ratios of $\mu_{N_2} = 0.97$, $\mu_{CH_4} = 0.03$, and $\mu_{CO} = 0.00046$ for computing the heating and cooling rates. The energy fluxes and effective cross section for FUV absorption by CH_4 and EUV absorption by N_2 are given in Krasnopolsky (1999) for the various levels of solar activity at Pluto's perihelion (i.e. 30 AU). We obtain globally averaged heating rates for the FUV/EUV by applying Lambert-Beer's Law for a plane-parallel atmosphere separately for each species s: $F_s(r) = \frac{1}{2}\mu F_s^\infty \exp(-\tau_s(r)/\mu)$, where $F_s(r)$ is the energy flux, $\tau_s(r) = \int_r^\infty \sigma_s n_s(r)dr$ is the vertical optical depth, σ_s is the cross section of species s, n_s is the number density of species s, and $\mu = \cos(60°) = 0.5$ is used to approximate spherically averaged heating (Strobel and Zhu, 1996; Apruzese, 1980). Then the heating rate for each species is given by

$$q_s(r) = \frac{dF_s}{dr} = \frac{\sigma_s n_s(r)}{\mu}F_s(r) \tag{7}$$

Further heating and cooling is provided by methane near-IR absorption and CO rotational line emission both of which are non-LTE processes. Parameterizations of these processes are given in Strobel (2008), fit to the detailed radiative-transfer model of Pluto's lower atmosphere Strobel and Zhu (1996). The methane heating rate per molecule is given as $8 \times 10^{-22}\exp(-\frac{\lambda-\lambda_0}{1.6})$ ergs per sec, where $\lambda = \frac{GMm}{rk_bT_0}$ and $\lambda_0 = \lambda(r_0)$. The CO rotational cooling rate per molecule is given as $8 \times 10^{-20}(\frac{T}{105})^{2.45}$ ergs per sec.

These calculations assume a fixed efficiency for the various processes, yet we know that this assumption will break down when the gas becomes tenuous. To accommodate this we assume that above $Kn = 0.1$ the heating is zero (i.e. efficiency drops to 0). Further, with the heating per molecule constant, including heating up to the top boundary can cause numerical instability even though the heating rate per unit volume is small. In describing the heating, a cut-off is often used where the tangential line of sight is unity Strobel (2008), which in our case lies below the $Kn = 0.1$ level.

Previously we directly solved the time-independent equations, iteratively solving them along with the heating and the DSMC escape simulations until a consistent solution is found (Tucker et al., 2012; Strobel, 2008). Here we reintroduce the time-dependence into the energy equation and time-step until convergence. This is found to be more numerically stable for the boundary conditions that we will use here. We make the substitution $\xi = T^{s+1}$ as in (Strobel and Zhu, 1996; Zalucha et al., 2010) in the Eq. (6) to obtain a linear time-dependent PDE:

$$\frac{d\xi}{dt} = \frac{(s+1)T^s}{nC_p}\left(q(r) - \frac{\phi}{4\pi r^2}\frac{d}{dr}\left(\frac{1}{2}mu^2 - \frac{GMm}{r}\right)\right)$$
$$+ \left(\frac{\kappa_0 T^s}{nC_p}\frac{2}{r} - \frac{\phi}{4\pi r^2 n}\right)\frac{\partial\xi}{\partial r} + \frac{\kappa_0 T^s}{nC_p}\frac{\partial^2\xi}{\partial r^2} \tag{8}$$

This equation is solved using the finite differences and the implicit, time-stepping scheme described in Appendix A. This second-order equation needs two boundary conditions, the first is the fixed lower boundary temperature $T(r_0) = 88.2K$. The second is a restriction on the energy flux leaving the atmosphere

$$4\pi r^2\frac{\kappa_0}{s+1}\frac{d\xi}{dr}\bigg|_{r_{top}} = \phi\left(C_pT - \frac{GMm}{r}\right)_{r_{top}} - \phi_E \tag{9}$$

3

This condition is derived by integrating Eq. (6) from the exobase to the upper boundary, and using ϕ_E for the energy flux at the exobase.

The time stepping advances the temperature alone, next we find density, n, and bulk velocity, u, at the new time step. First u is updated using Eq. (4) and the previous n. This new value of u is used to update n using the momentum equation (5) expressed as

$$n(r) = n_0 \exp\left(-\int_{r_0}^{r} \frac{\frac{d}{dr}(k_b T + \frac{1}{2}mu^2 - \frac{GMm}{r})}{k_b T} dr\right) \qquad (10)$$

As these two equations are coupled through n and u, we iteratively solve them together to find a consistent solution. A few iterations are sufficient to get the fully consistent solution for T, n, and u. With these profiles determined, the heating components are recalculated.

We proceed with the time stepping in two ways. As in Tucker et al. (2012), we use the previous DSMC values of ϕ and ϕ_E and time-step until the solutions are consistent with these values. Then we run a new DSMC simulation from values obtained where the Knudsen number $Kn = 0.1$. This is far enough below the exobase, in the collision-dominated regime, to act as a lower boundary for the single component DSMC simulation, and above which heating can be ignored. The DSMC results for escape ϕ and ϕ_E are then used in the next fluid solution. After a few exchanges between the fluid and DSMC models, a consistent solution is found for each specific heating case. Although non-thermal processes in the exobase region contribute to and can dominate the atmospheric loss rate, we ignore these here, consistent with previous work on escape from Pluto. Such processes will be included in subsequent work.

Because the DSMC calculations can be time consuming, for comparison, we also approximate the escape process as Jeans-like. That is, in each iteration we find the exobase, $Kn = 1$, and compute the Jeans escape values (including bulk velocity) for ϕ and ϕ_E for the next time-step. A consistent solution is obtained by stepping in time. Since we have shown earlier using the molecular kinetic model that the Jeans rate consistently underestimates the escape rate for the range of λ of interest here, we also scale the Jeans escape rates by a value ~2 consistent with our earlier DSMC results.

The Jeans escape boundary condition have been used in modeling planetary atmospheres, notably by Chassefière (1996), Yelle (2004) and Tian et al. (2008). In modeling the response of Earth's thermosphere to EUV heating, Tian et al. used the Jeans escape expression to determine the velocity at the upper boundary with the upper boundary being the exobase, but fixed the heat gradient at the upper boundary for the energy equation. In modeling extra-solar gas giants at small orbital distance, Yelle also used Jeans escape, with a drifting Maxwell-Boltzmann velocity distribution, to get an upper boundary velocity. But Yelle applied this at a fixed upper boundary of 3 planetary radii rather than at the exobase.

To aid in convergence to steady-state, we estimate the heating q at the advanced time step using a Taylor expansion in ξ as $q(r, \xi^{i+1}) = q(r, \xi^i) + \frac{dq}{d\xi}(\xi^{i+1} - \xi^i)$. This can help dissipate numerical oscillations between time steps, speeding up convergence. In calculating the derivative for the FUV and EUV heating we assume $\frac{dn}{dT} = 0$ and $\frac{d\tau}{dT} = \frac{\tau}{T}$ as the optical depth $\tau \approx \sigma n H$ with H depending linearly on T.

The lower boundary is set at 1450 km, consistent with the occultation results and with the assumptions in Strobel (2008). Since we showed earlier that the atmosphere is highly extended, the upper boundary is set to 16000 km to accommodate the solar maximum case. For the radial grid, we need a fine resolution for the first 3000 km where the heating occurs, but a coarse grid is sufficient above this. Therefore, we use a grid that is equally spaced in $1/r$. With 1600 points in r we get a lower boundary dr of order 1 km and an upper boundary dr of order 100 km.

3. Results

3.1. Fluid-DSMC

With the time-dependent solver, which is an improvement on the steady-state iterations used in Tucker et al. (2012), we are able to model higher solar heating rates. We present the two solutions found in that paper for no heating and solar minimum heating along with a new fluid-DSMC hybrid result for solar medium heating in Figure 1. This allows us to bracket the expected heating rates at the NH encounter. The hybrid solution includes rotational/ translational energy exchange consistent with the assumed thermal conductivity (see Tucker et al. (2012)).

Looking at Figure 2, a few qualitative differences between the hydrodynamic solutions and our fluid-DMSC solutions are seen. Although the two types of calculations give similar escape rates, they produce different temperature profiles also discussed in (Volkov et al., 2011; Tucker et al., 2012). In the DSMC the parallel and perpendicular temperature differ above $Kn \approx 0.1$. More important for the NH encounter, the exobase altitude for the fluid-DSMC is much higher suggesting a significantly
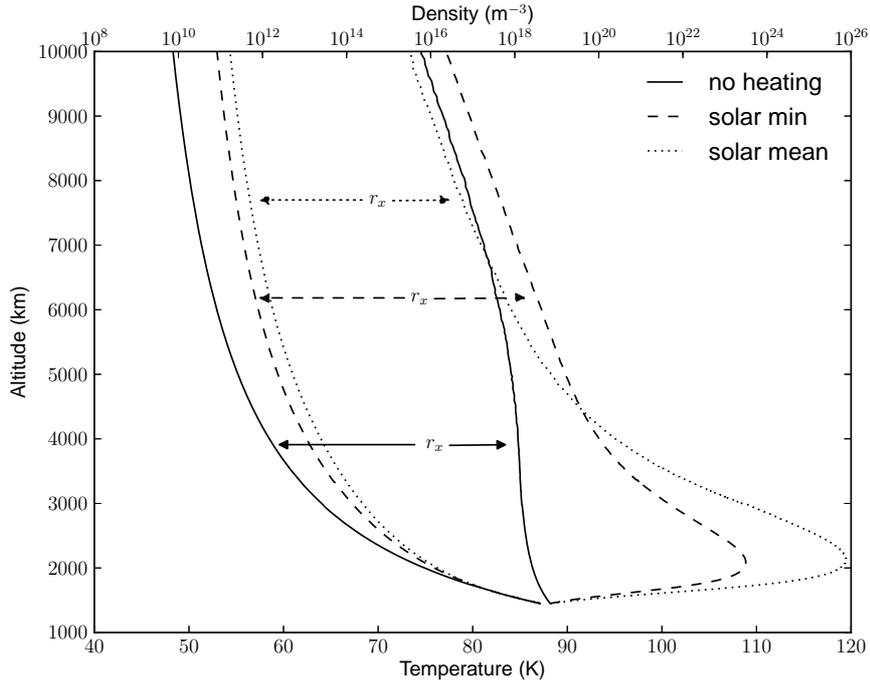
Figure 1: Temperature (right) and density (left) profiles for the hybrid fluid-DSMC model of Pluto, for the special cases of no heating and solar minimum (from Tucker et al. (2012)), and our new result for solar medium. The temperate profiles are plotted with the scale labeled below; the density profiles are plotted on a logarithmic scale, with scale labeled above. The exobase altitudes are marked for each case.
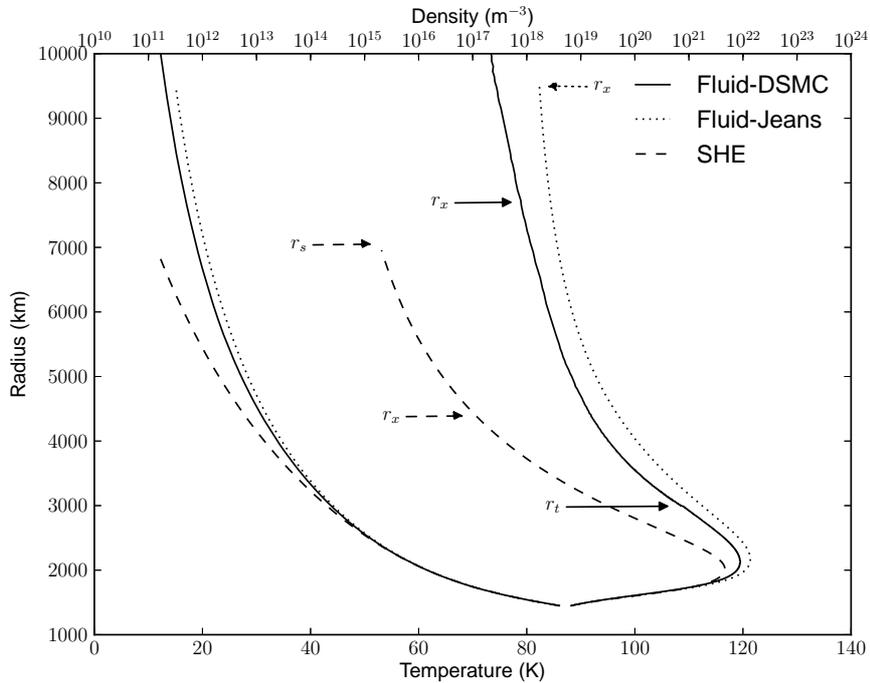

Figure 2: Temperature (right) and density (left) profiles for solar medium-like condition, comparing the fluid-DSMC solution of this study with that of SHE from Strobel (2008), along with the fluid-Jeans solution describe in Section 3.2. Marked on the fluid-DSMC solution is the exobase (r_x) as well as the transition between the fluid model and DSMC (r_t, where $Kn(r_t) = 0.1$). Marked on the SHE model are the exobase (r_x) and the sonic point (r_s).

more extended atmosphere for Pluto. Further, the hydrodynamic methods can produce an atmosphere that expands faster than the sonic speed. However, we find the expansion is subsonic with the bulk flow being less than 3% the speed of sound at the exobase. Further out, the bulk speed increases to approach a nearly constant value well below the speed of sound, consistent with a Jeans-like model.

In the solar medium case, the transition from the fluid to DSMC domain is near 3000 km. In the region $0.1 < Kn < 1.0$ the agreement between the fluid and the DSMC is better than 5% as in Tucker et al. (2012). The DSMC solution begins to deviate from the fluid solution near the altitude at which the kinetic and internal energies of the molecules begin to separate, which is associated with the transition to non-equilibrium flow. It is important to note that this occurs below the exobase, so that the region of validity of the fluid equations should be terminated below the exobase. Our choice of $Kn = 0.1$ for connecting the DSMC solution to the fluid solution is at an altitude below which this separation occurs.

Strobel (2008) solutions result in exobase levels much lower than that found in our model. The corresponding exobase altitudes are ~0.56 - 0.7 of those calculated with the hybrid model. With these lower altitudes and the lower temperatures, the Jeans parameter at the exobase, λ_{exo}, are ~2.6 - 3.3 times larger than found in this study. Using these high λ_{exo} in Eq. (2) the Jeans escape rate is significantly lower than the escape rate found; hence the earlier conclusion that escape rates were orders of magnitude larger than the Jeans rate. In contrast the fluid-DSMC model results in an escape rate that is only modestly enhanced relative to the calculated Jeans rate, the ratio $\phi/\langle\phi\rangle_J$ being 1.6, 2.0 and 2.3 for the cases considered.

	none	min	med
Q (10^{14} ergs per sec)	0	3.8	7.8
ϕ (10^{27} per sec)	0.047	1.20	2.56
E_{esc} (10^{-3} eV)	14.6	14.3	14.3
r_{exo}/r_p	3.37	5.24	6.71
λ_{exo}	8.9	5.7	4.8
$\phi/\langle\phi\rangle_J$	1.6	2.0	2.3
ϕ/ϕ_L	-	.88	.91
$E_{esc}/\langle E_{esc}\rangle_J$	.95	.90	.97

Table 1: Fluid-DSMC results. $E_{esc} = \phi_E/\phi$ is the average energy carried off per molecule; r_{exo} is given as a ratio to $r_p = 1150$ km. $\langle\phi\rangle_J$ is computed using exobase values from the solution, $\phi_L = Q/U(r)$ is computed using Q from the solution and $r = 1450$ km.

The results in Figure 1 and Table 1 correspond to a net solar heating/cooling $Q = \int_{r_0}^{r_x} 4\pi r^2 q(r)dr$ of 0.0, 3.8, and 7.8 $\times10^{14}$ ergs per sec. These can be compared to 0.0, 3.4, and 6.9 $\times10^{14}$ ergs per sec found in Strobel (2008). To give context for these heating rates, the upward flow of energy across Pluto's 1450 km level is greater than 10^{20} ergs per sec if it were escaping hydrodynamically (i.e. $\lambda \to 0$).

Table 1 gives many of the relevant values of the fluid-DSMC hybrid solution in Tucker et al. (2012) including the new solar medium-like case calculated here using the time dependent model iteratively with a DSMC calculations. It is seen that the escape fluxes are comparable to the Jeans flux and are also, quite remarkably, comparable to our estimate of the energy limited rate with the exception, of course, of the $Q = 0$ case. This result alone is important, as it is often presumed that the Jeans rate and the energy-limited rate are two limiting cases for atmospheric loss.

As in Tucker et al. (2012), for no heating our escape rate is a order of magnitude lower than the SHE solution. For solar minimum we are 20% below the SHE solution, and for solar medium we are slightly above. In each of these cases we deposit somewhat more heat than in Strobel (2008) due to differences in atmosphere structure. Scaled to the same heating rates the fluid-DSMC escape rate would be somewhat smaller than the hydrodynamic model as the DSMC produces higher temperatures in the exosphere region.

3.2. Fluid-Jeans

The fluid-DSMC solutions demonstrate that the escape rate and energy escape rate are within a factor of the order of unity of the Jeans rate calculated from Eqs. (2) and (3) using the temperature at $Kn = 1$. Therefore, in Figure 2 and Table 2 we present results using an upper boundary condition that is equal the Jeans escape and energy loss rates, and then doubling those. It is seen that the fluid-Jeans solution is in many respects close to that of fluid-DSMC. Therefore, for Pluto's atmosphere under solar heating conditions likely occurring at the NH encounter, approximating the escape process as Jeans-like reproduces many of the properties of the full solution that we are interested in. Although the fluid equations may not be exact up to the exobase, using them along with Jeans escape boundary conditions allows us to carry out parameter studies that are impractical with the full fluid-DSMC model.

From Table 2 we note that the escape rate is consistent with the fluid-DSMC model, but the other properties of the atmosphere differ, and this difference increases as the heating rate increases. The atmosphere is more extended
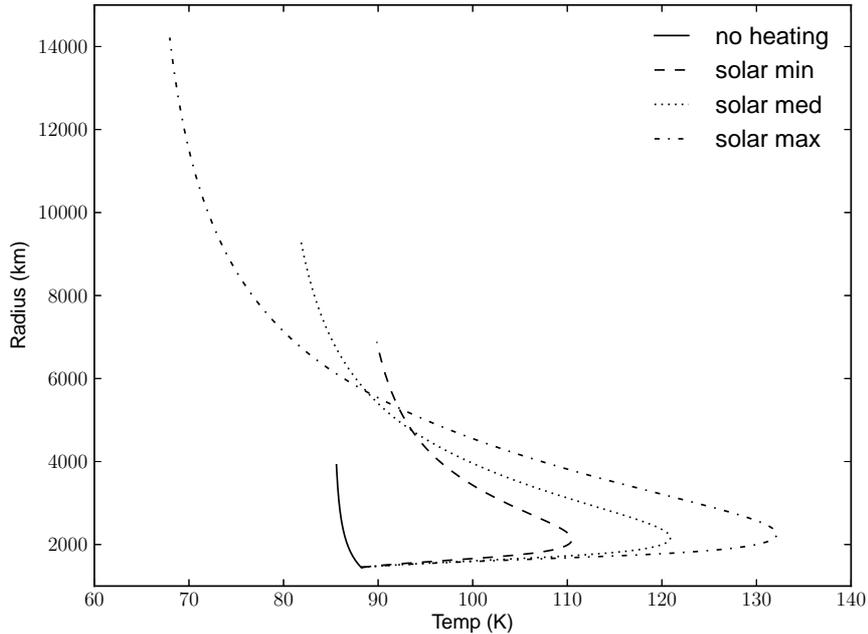
Figure 3: Temperature profile found in the fluid-Jeans model for the 4 special cases discussed: no heating, solar minimum, solar medium, and solar maximum. The top of each curve represents the exobase altitude.

than in the fluid-DSMC model, allowing it to absorb more EUV heating. The Jeans parameter at the exobase is lower than that found in the fluid-DSMC model, which also can be attributed to the more extended atmosphere.

In an attempt to more accurately model escape based on the DSMC we also used $\phi = 2 \times \langle \phi \rangle_J$ and $\phi_E = 2 \times \langle \phi_E \rangle_J$ for the boundary condition (note that the energy per molecule, E_{esc}, is unchanged by this scaling as found in the fluid-DSMC results). The most notable effect of this is to lower the exobase altitude and increase λ_{exo}. These results now more closely resemble the fluid-DSMC results in Table 1. Surprisingly, ignoring the no heating case, the converged escape rate is barely affected by the enhancement of the Jeans boundary conditions. The same statement applies if we increase the enhancement to 3 or 4 times Jeans. Since the escape rate is roughly given by the energy-limited approximation, this is consistent with the loss rates being insensitive to the size of the enhancement in the Jeans boundary conditions. Therefore, the other properties of the atmosphere adjust to ensure this. However, we would not have had an estimate of the enhancement of the escape rate relative to Jeans in the absence of the fluid-DSMC simulations. Our early DSMC simulations indicated that for the case of no heating above the lower boundary of the simulation region, the enhancement is ~1.6 (Volkov et al., 2011). How it increases with heat-

ing remains an open problem.

As we increase the heating and the atmosphere gets further extended, the Jeans parameter decreases to about 3 at the exobase for the solar maximum case using the Jeans boundary conditions. This is within the region that Volkov et al. (2011) found that marks the transition to hydrodynamic escape for N_2 at the relevant temperatures. In that study, it was shown that for the lower boundary at small Kn, the exobase moves out to infinity as the Jeans parameter approaches 3. Using twice the Jeans expressions in Eqs. (2) and (3) as the boundary conditions, the Jeans parameter in the upper atmosphere increases keeping the solution from entering the transonic regime.

Based on the enhancement versus heating rate found in Table 1, we estimate the actual enhancement for solar maximum condition to be close to 3.0 times the Jeans rate. If we accept the assumption that the enhancement will be 3.0 times Jeans for the solar maximum case then we can use the fluid-Jeans model to discuss the atmosphere. From Table 3 we observe the heating rate has about doubled relative to solar medium, and the escape rate has slightly more than doubled. The average energy carried off per particle has decreased by ~30% relative to solar medium, but this is a property of the fluid-Jeans model that isn't representative of the fluid-DSMC model. The energy limited escape rate $\phi_L = 5.61 \times 10^{27}$ for this Q, using $U(r_0)$,

7

Using 1× Jeans			
	none	min	med
Q (10^{14} ergs per sec)	0	3.86	7.87
ϕ (10^{27} per sec)	0.035	1.14	2.58
E_{esc} (10^{-3} eV)	15.5	16.3	14.6
r_{exo}/r_p	3.41	5.99	8.10
λ_{exo}	8.71	4.72	3.84
Using 2× Jeans			
	none	min	med
Q (10^{14} ergs per sec)	0	3.83	7.79
ϕ (10^{27} per sec)	0.054	1.17	2.58
E_{esc} (10^{-3} eV)	15.2	15.4	13.7
r_{exo}/r_p	3.34	5.30	6.84
λ_{exo}	9.02	5.55	4.72

Table 2: Results of fluid model using Jeans-like escape from the exobase. First results using Jeans escape values for ϕ and ϕ_E, while the second set uses twice the Jeans values to better capture the enhancement of escape relative to Jeans. r_{exo} is given a ratio relative to $r_p = 1150$ km.

solar maximum			
	1×	2×	3× Jeans
Q (10^{14} ergs per sec)	15.8	15.7	15.6
ϕ (10^{27} per sec)	5.81	5.80	5.79
E_{esc} (10^{-3} eV)	11.7	10.9	10.4
r_{exo}/r_p	12.4	9.8	8.9
λ_{exo}	3.01	3.95	4.48

Table 3: Results for fluid-Jeans model for solar maximum case. Given are results for 1×, 2×, and 3× the Jeans value as a boundary condition. This last value is an estimate of the enhancement that would result from DSMC models, inferred from the results in Table 1.

is close to our estimated escape rate.

In Figure 3 we plot the results for the four cases considered here using the Jeans criteria in Eqs. (2) and (3) at the upper boundary. The no heating case was initiated using an isothermal profile and time stepped to steady state. Then we incrementally increased the solar flux rates to obtain the other 3 profiles in turn. As the exobase altitude increased with heating rate, the upper boundary altitude had to be increased resulting in our use of 16000 km, about $14r_p$, to model the solar maximum condition as discussed earlier. We see that unlike the exobase level, the altitude of the peak in the temperature does not increase significantly with heating rate, changing from 2124 km to 2250 km from solar minimum to solar max with temperatures of 110K and 132K respectively. The heating peak is below the temperature maximum, and also does not change significantly with heating rate, going from 1767

km to 1780 km. This heating peak is near where the optical depth of the CH_4 FUV is unity. The solutions become nearly isothermal at the exobase consistent with the fluid-DSMC model, but different from the Parker (1964) and slow-hydrodynamic models (McNutt, 1989; Watson et al., 1981; Krasnopolsky, 1999; Strobel, 2008) that require the temperatures to decrease to zero.

In his fluid dynamic studies of an early Earth atmosphere using the Jeans rate for the upper boundary conditions, Tian et al. (2008) found two regimes of escape in in response to increased UV heating. The transition from hydrostatic equilibrium to what he calls hydrodynamic escape coincides with adiabatic cooling becoming non-negligible when compared to conduction or radiative heating. In our simulations for Pluto, adiabatic cooling is always an important cooling mechanism in the upper atmosphere. Further, we find similar changes in exobase altitude, temperature and bulk velocity with increased heating as in that paper's hydrodynamic escape regime, even though our escape is described as a kinetic process. That adiabatic cooling is always important in our simulations is likely due to the much smaller gravitational binding energy and the similarities mentioned are likely due to his use of the Jeans escape rate at the upper boundary, which we showed here can be a reasonable approximation to the kinetic boundary conditions.

In Figure 4 we compare the escape rate versus the net heating for the fluid-Jeans model to the other calculations. The fluid-DSMC results are nearly the same, confirming that the fluid-Jeans model can be used to estimate the escape rate for this range of Jeans parameter. With the exception of the no heating case, the SHE model results show a similar trend but are 43%, 16% and 7% higher than the fluid-Jeans for solar minimum, medium, and maximum respectively, with the latter approaching blow-off.

Also shown in Figure 4 is the energy-limited escape rate compared to our escape rate. The good agreement between the two suggests that most of the energy being deposited is going into removing the molecules from the gravitational well. The sources of cooling besides adiabatic expansion and loss to escape are conduction through the lower boundary and CO cooling (already included in Q), both of which are bounded, as found in the hydrodynamic model (Strobel, 2008). The slope of the energy-limited escape rate can be better matched to our simulations by including the internal energy (i.e. $C_p(T_0 - T_{exo})$) in the denominator, and the vertical offset can be partly compensated for by subtracting the loss to conduction from the total energy deposited.

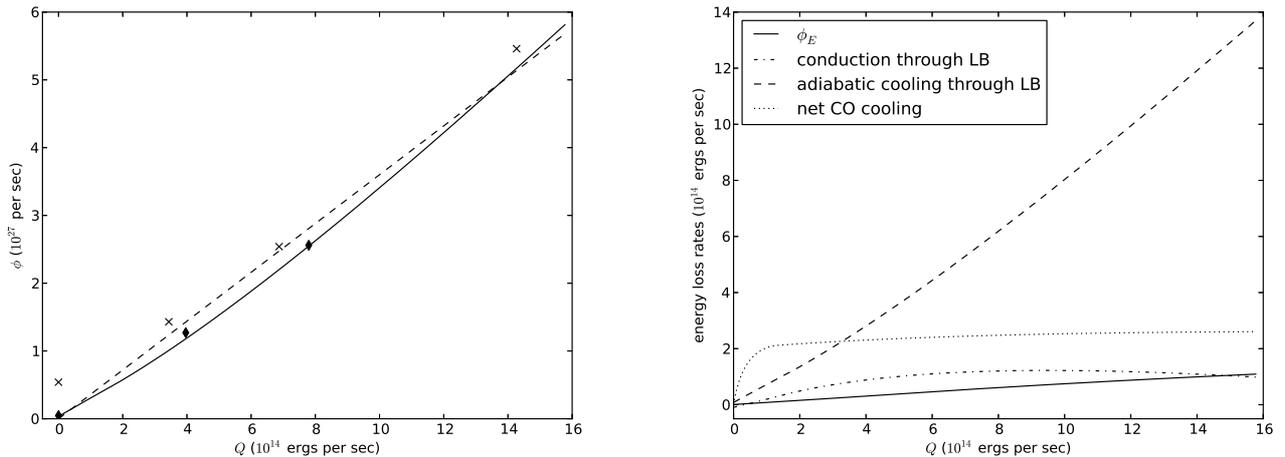We also compared estimates of the hydrodynamic

Figure 4: (Left) Escape rate ϕ (solid line) plotted versus net heat deposited Q from the fluid-Jeans model. Overlaid are escape rates from the fluid-DSMC model as black diamonds, and from the SHE model (Strobel, 2008) as x's. Also plotted is the energy limited escape rate $\phi_L = Q/U(r_0)$ (dashed line). (Right) Comparing energy loss mechanisms versus net heat deposited from the fluid-Jeans model.

escape rates in Hunten and Watson (1982) and McNutt (1989), and the energy-limited escape rate Lammer et al. (2009) for the same solar flux. We calculated the heating by CH_4 assuming a fixed mixing ratio of 3%, a globally averaged incoming solar energy flux, $S = \eta F$, of 1×10^{-3} and 4×10^{-3} ergs per cm^2 per sec (representing near solar minimum and maximum conditions respectively), an absorption cross-section for CH_4 of 1.8×10^{-17} cm^2, and primarily nitrogen atmosphere with the values for conductivity used in this paper.

From Table 4 we see that neither of the simple hydrodynamic models produces a similar estimate to the fluid-Jeans model for either heating case. The Hunten and Watson (1982) model is an upper bound, so it consistently overestimates the escape rate. The McNutt (1989) is a good estimate for the smaller heating case, giving a similar estimate of both escape rate and where the heating layer occur, but is quite different for the strong heating case. While these models can give good estimates of the escape rate for some cases, the solutions for the structure of the atmosphere are quite different from that found using our hybrid fluid-kinetic model.

The energy-limited escape model is quite good if one knows the net heat deposited in the atmosphere, which depends on the atmospheric size. But without detailed modeling, one can only estimate the amount of energy lost through conduction and escape or deposited via heating. In Table 4 we consider using the energy-limited escape model with 4 estimates of the net heat deposited. First we use the net heating found from the fluid-Jeans model, then used $Q = \pi r_h^2 S$ with the location of the heating layer be-

ing the location of unity, parallel or vertical, optical depth (these altitude could also be estimated from observation), and finally with the heat deposit at the lower boundary as if no estimate were available. Knowing the net heating or the location of the heating layer provided a good estimate for the highly heating case, but for the near solar minimum case both overestimate the escape as a significant amount of heat is conducted through the lower boundary. Using the parallel optical depth provides a better estimate of the heat deposited.

We investigated the sensitivity of the model to changes in some model parameters. If the atmosphere were a monatomic gas ($C_p = 5/2 k_b$), then E_{esc} is about halved, primarily due to no internal energy being carried off, but the other properties are only significantly affected when the heating exceeds solar medium conditions. For solar medium, the escape rate increases by ~10% and the exobase is lower by a few hundred kilometers. In hydrodynamic models it is often assumed that the energy carried off by escape is negligible and a positive non-zero value can only decrease the escape rate. If we use $\phi_E = 0$ (keeping ϕ as the Jeans value), then the escape rate increases by ~5-10%. When the solar heating is above solar medium, corresponding to when ϕ_E normally becomes a comparable energy loss process to conduction or CO cooling, the exobase altitude is lowered and the exobase temperature raised by as much as 20%. Therefore, even though neglecting ϕ_E still produces a good estimate of escape rate, it should be included when interested in the structure of the atmosphere.

Another consideration is our definition of Knudsen

9

| $S = 1 \times 10^{-3}$ ergs cm^{-2} sec^{-1} | | |
	ϕ (10^{27} s^{-1})	r_h/r_0	Q (10^{14} ergs s^{-1})
Fluid-Jeans	1.06	1.22	4.68
Watson	15.4	3.66	35.4
McNutt	0.84	1.17	3.69
ELE (a)	1.69	-	4.68
ELE (b)	1.66	1.32	4.62
ELE (c)	1.41	1.22	3.94
ELE (d)	0.95	1.0	2.64
$S = 4 \times 10^{-3}$ ergs cm^{-2} sec^{-1}		
	ϕ (10^{27} s^{-1})	r_h/r_0	Q (10^{14} ergs s^{-1})
Fluid-Jeans	8.46	1.25	23.3
Watson	32.1	2.73	76.8
McNutt	3.22	1.28	17.4
ELE (a)	8.40	-	23.3
ELE (b)	7.30	1.39	20.3
ELE (c)	5.91	1.25	16.4
ELE (d)	3.81	1.0	10.6

Table 4: Comparing the fluid-Jeans model, Hunten and Watson (1982), McNutt (1989) and energy-limited escape (ELE). The values for each given are the escape rate ϕ, the location of the heating layer in terms of the lower boundary r_h/r_0 (in the case of the fluid-Jeans model we give the location of the peak heating, which is also the unity verticle optical depth), and the net heating Q. The ELE model was applied in 4 ways: (a) using Q from the fluid-Jeans model, (b) r_h is altitude of unity parallel optical depth, (c) r_h is r_{EUV} from the fluid-Jeans model, (d) and r_h is r_0 as if no estimate were given.

number used to determine the exobase. The relevant scale length in atmosphere is determined by the density gradient as $H_n = -n/(dn/dr)$. In the above simulations we have used the isothermal approximation $H = k_b T/mg(r)$. Using $Kn = \ell/H_n$ to determine the exobase results in a small correction (as $H \simeq H_n$ though out the atmosphere) and has a negligible effect on the solution and escape rate. Since our atmosphere is highly extended one might consider $Kn = \ell/r$, which is appropriate for comets, where the density drops off rapidly as $1/r^2$. Using this definition, the exobase altitude increases to 4.7, 9.3, 13.3, and 21.6 times r_p for special cases. These values are about 50% larger as compared to those in Table 2 and 3. For solar maximum such an estimate would place the exobase beyond the orbit of Charon.

3.3. Similar Escape Rates for Small Jeans Parameters

This study has shown that the escape rates of the fluid-Jeans and fluid-DSMC are close to those found in the hydrodynamic models when there is heating, and become closer as the heating increases. We posit that this can be explained by the Jeans parameter being lowered at the upper boundary of the heating layer, and that for small Jeans parameter only a small range of escape rates lead to valid solutions as discussed below.

In Figure 5 we plot the escape rate versus Jeans parameter at the lower boundary for various models of escape. For these calculations, we rewrite the fluid equations in a non-dimensional form, where the lower boundary conditions are given by the Knudsen number, Kn_0, the Jeans parameter, λ_0, and the Mach number (scaled to the isothermal speed of sound), Ma_0, as shown in Volkov et al. (2011). In Figure 5 we compare the Parker (1964) solution, which is the critical transonic solution that the many hydrodynamic models are based upon, to the fluid-Jeans solution of this paper. Also shown is the escape rate given by Gruzinov (2011) in his analytic solution to these equations. These were shown to match well with the transition in escape rate found in the DSMC simulations of Volkov et al. (2011).

We see that the Parker and fluid-Jeans solutions begin to converge as the Jeans parameter decreases. As we increase the heating, the atmosphere expands and the Jeans parameter above the heating layer is decreasing, so the two models should produce similar escape rates. The fluid-DSMC solution lies between the Parker and fluid-Jeans as it is enhanced relative to Jeans but not a sonic solution.

Solutions to the full hydrodynamic equations of Parker (1964) can be very sensitive to the escape rate, especially as the Jeans parameter decreases, and not all choices of escape rate can lead to valid solutions. The shaded region in Figure 5 gives the range of escape rates that support an exobase. The most important feature of this region is the change from containing static solutions, $Ma_0 = 0$, to becoming narrow for small values of Jeans parameter.

Both the fluid-Jeans and Parker's solution lie within this region, as does the slow-hydrodynamic escape solution. Then for both solutions to have an exobase, they must have similar escape rates for small Jeans parameters. As stated above, even though the escape rates are within a factor of order unity, the upper atmosphere can have very different structures, from a super-sonic, rapidly cooling solution, to the near isothermal solution near the lower edge of the narrow region.

When the atmosphere is heated this argument must be applied above the heating layer. Applying this at $Kn_0 = 0.1$, where we have cut-off the heating, the narrow region occurs for $\lambda_0 < 6.7$. We find that this value is achieved near solar medium heating. Therefore for solar medium and maximum heating the slow-hydrodynamic
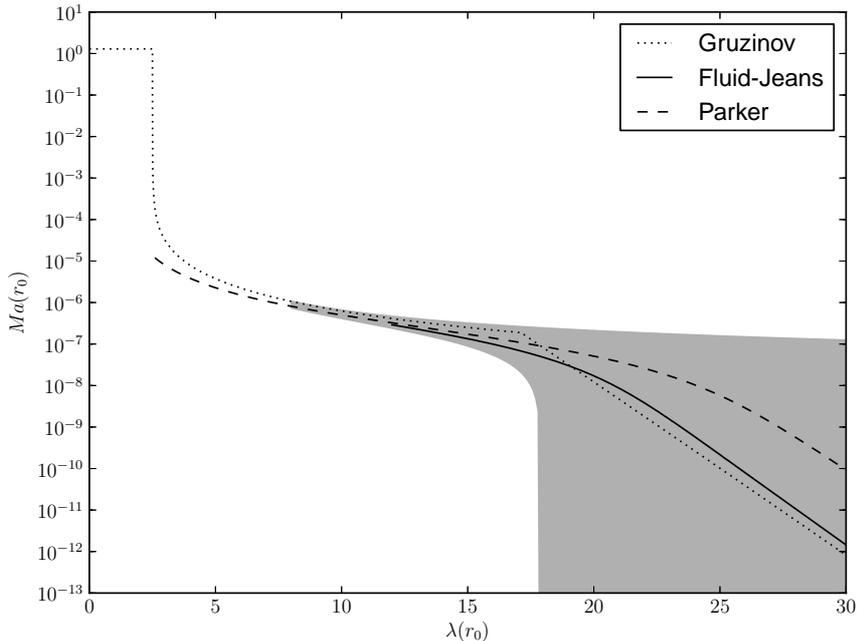
Figure 5: Solutions from Gruzinov (2011) and Parker (1964), compare to our fluid-Jeans solutions without heating for $Kn_0 = 10^{-5}$ (about Pluto's 1450 km value). The shaded region is the range of escape rates that support an exobase.

escape model and our hybrid models produce similar escape rates, even though the solutions are very different in describing the extended atmosphere.

4. Conclusion

We compared two methods for modeling the upper thermosphere and characterizing escape. Having shown earlier that such models can be scaled Volkov et al. (2011), we considered Pluto's atmosphere as an example because of the anticipated NH encounter. We found that, in the presence of significant heating, the escape rate did not change significantly from that obtained in certain fluid models. However, many other characteristics of the atmosphere are affected, namely the exobase altitude and the existence of a sonic point.

Since the fluid-DSMC model described earlier requires no assumption on upper boundary conditions, we used this as a base line for testing fluid models that require assumptions about the particle and energy flux at the upper boundary. By iteration, the escape rate and energy escape rate were shown to be continuous throughout the simulation domain as were the density, temperature and flow speed. We obtain a solution out to 10's of planetary radii. The escape rate found is approximately 2 times Jeans, but this value changes slowly with the amount of

heat deposited in the upper atmosphere, as well as with the temperature at the lower boundary of the simulations, as shown earlier. The arrival of New Horizons should occur when the FUV/EUV flux is between the solar minimum and medium cases considered in this paper.

The fluid-Jeans model uses the upper boundary conditions for Jeans escape as an approximation to use of the DSMC model in the exobase region. It was shown that the resulting escape rate is close to that given by the fluid-DSMC model. But we also show here that the small differences in escape rates do not imply that the temperature and density structures are similar. By scaling the Jeans escape rate by a factor between 2 and 3 the results become closer to the Fluid/DSMC.

We also showed that the energy limited escape rate, often used for estimating atmospheric loss from exoplanets, was surprisingly accurate over a broad range of heating conditions. Since the details of the atmospheric structures of exoplanet atmospheres are usually not known, we also show that in applying this estimate one should use a radius associated with the FUV/EUV absorption depth or, better, use that depth at which the parallel optical depth is unity. This depth can be roughly estimated by scaling to the visible radius using the ratio of the cross sections, the visible light scattering cross section to the FUV/EUV absorption cross, along with a scale height es-

11

timated using the equilibrium temperature. In this way the results here can be applied when modeling the evolution of exoplanet atmospheres.

For the heating rates considered here we have not seen the transition from Jeans-like to hydro-like escape. However, the resulting highly extended atmosphere for NH encounter conditions means that the direction of the modeling effort for Pluto needs to change. That is, in thermal escape calculations one terminates the energy deposition at very high altitudes as the heating efficiency of the background gas due to solar radiation absorption drops rapidly with increasing altitude in the exobase region. However, the molecules in this the upper regions of this highly extended atmosphere *do absorb* radiation. Although this might not efficiently heat' the atmosphere, a fraction of it does produce non-thermal escape, as described for other bodies (Johnson et al., 2008). In addition, the interaction with the solar wind will now occur at much larger distances from Pluto than had been predicted and can more efficiently strip the atmosphere (see Bagenal and Mcnutt (1989)). For the extended atmosphere described here, these non-thermal processes at the NH encounter conditions could be comparable to thermal escape estimates and determine affect the NH observations. Such modeling is now in progress.

Ackowledgements

Appendix A. An implicit time stepping scheme with varying step size

In this appendix, we describe the numerical equations and techniques used to solve the diffusion equation on an unequally spaced grid. We define the grid r_m, $m = 1, \ldots, M$ and a spacing $\Delta r_m = r_{m+1} - r_m$. Define $\overline{\Delta r_m} = (r_{m+1} - r_{m-1})/2$ as the average spacing at grid point r_m. Last define ξ_m as the finite difference approximation to $\xi(r_m)$.

First we describe approximate the derivatives $d\xi/dr$ and $d^2\xi/dr^2$ using unequal spacing. Using the points $\xi_{m+1}, \xi_m, \xi_{m-1}$ to approximate $d\xi/dr$, one might use the center difference scheme $\xi'(r) \approx (\xi_{m+1} - \xi_{m-1})/(2\overline{\Delta r})$. But this scheme is not second order accurate, $O(\overline{\Delta r}^2)$, as it

would be in the case of equal spacing. The correct error term is proportional to $(\Delta r_m - \Delta r_{m-1})\xi''(\tilde{r})$. While the quantity $(\Delta r_m - \Delta r_{m-1})$ might be small compared to $(\overline{\Delta r_m^2})$, the effect of this error in the model is to over-estimate the conductivity. To correct for this we use the finite differences:

$$\xi'(r) = \frac{1}{2}\left(\frac{\Delta r_{m-1}}{\Delta r_m \overline{\Delta r_m}}\xi_{m+1} + \frac{2(\Delta r_m - \Delta r_{m-1})}{\Delta r_m \Delta r_{m-1}}\xi_m - \frac{\Delta r_m}{\Delta r_{m-1}\overline{\Delta r_m}}\xi_{m-1}\right) \tag{A.1}$$

$$\xi''(r) = \left(\frac{1}{\Delta r_m \overline{\Delta r_m}}\xi_{m+1} - \frac{2}{\Delta r_m \Delta r_{m-1}}\xi_m + \frac{1}{\Delta r_{m-1}\overline{\Delta r_m}}\xi_{m-1}\right) \tag{A.2}$$

The error term on ξ' is now $\Delta r_m \Delta r_{m-1}\xi'''(\tilde{r})$, now second order accurate and not affecting the conductivity. The error term for ξ'' is $(\Delta r_m - \Delta r_{m-1})\xi'''(\tilde{r})$. While the finite difference approximation for ξ'' is not second order accurate, this is the minimal error term one can get from the 3 points used. It is more important that we capture conduction correctly as to ensure a constant energy flux through the upper domain where there is no heating and the grid spacing is large.

We adapt the implicit scheme proposed by Zalucha et al. (2010), using the same notation, to solve the diffusion equation

$$\frac{\partial \xi}{\partial t} = S + B\xi + C\frac{\partial \xi}{\partial r} + G\frac{\partial^2 \xi}{\partial r^2} \tag{A.3}$$

on a domain $r \in (r_0, r_{top})$ along with the boundary conditions

$$\xi(r_0) = \xi_0 \tag{A.4}$$

$$\frac{d\xi}{dr}\bigg|_{top} = F_{top} \tag{A.5}$$

The coefficient B, C, G and source term S are functions of r and t. We make two modifications to the scheme. First we use our finite differences for unequal grid spacing, and second we modify the upper boundary condition to more accurately restrict the energy flow.

Implementing the time grid $t_i = i\Delta t$ for $i = 0, 1, \ldots$ and the notation $\xi(r_m, t_i) = \xi_m^i$. Our implicit scheme is now obtained by substituting the finite differences, Eqs. (A.1) and (A.2), evaluated at the advanced time step into the diffusion equation. For the time derivative we use $(\xi_m^{i+1} - \xi_m^i)/\Delta t$. Solving for the advanced time step then

requires solving a tridiagonal system of equations

$$\alpha_m \xi_{m-1}^{i+1} + \lambda_m \xi_m^{i+1} + \omega_m \xi_{m+1}^{i+1} = q_m \tag{A.6}$$

The lower boundary condition $\xi_1^i = \xi_0$ is then expressed as $\alpha_1 = 0$, $\lambda_1 = 1$, $\omega_1 = 0$, $q_1 = \xi_0$. The interior point (m = 2,...,M-1) are expressed as

$$\left.\begin{aligned}
\alpha_m &= \frac{\Delta t}{\Delta r_{m-1}\overline{\Delta r_m}}\left(\frac{\Delta r_m}{2}C_m - G_m\right) \\
\lambda_m &= 1 - \Delta t\left(B_m + \frac{1}{\Delta r_m \Delta r_{m-1}} \cdot \right. \\
&\qquad \left. ((\Delta r_m - \Delta r_{m-1})C_m - 2G_m)\right) \\
\omega_m &= \frac{-\Delta t}{\Delta r_m \overline{\Delta r_m}}\left(\frac{\Delta r_{m-1}}{2}C_m + G_m\right) \\
q_m &= \xi_m^i + \Delta t S_m
\end{aligned}\right\} \tag{A.7}$$

For the upper boundary we modify the procedure of interior points to enforce the condition on $\frac{d\xi}{dr}$ at the upper boundary. We substitute Eq. (A.5) in directly into Eq. (A.3) for the first derivative. Using the Eq. (A.2) with $m = M$ for the second derivative at the upper boundary introduces the phantom point ξ_{M+1}, but by equating Eq. (A.1) to Eq. (A.5) we can remove it from the equation. The result is expressed as

$$\left.\begin{aligned}
\alpha_M &= -\Delta t G_M \frac{1 + \Delta r_M/\Delta r_{M-1}}{\Delta r_M \Delta r_{M-1}} \\
\lambda_M &= 1 - \Delta t\left(B_M + G_M\frac{2 - \Delta r_M/\Delta r_{M-1}}{\Delta r_M \overline{\Delta r_M}}\right) \\
\omega_M &= 0 \\
q_M &= \xi_M^i + \Delta t\left(S_M + F_{top}\left(C_M + \frac{2}{\Delta r_{M-1}}G_M\right)\right)
\end{aligned}\right\} \tag{A.8}$$

References

Apruzese, J. P., 1980. The diffusion factor re-examined. Journal of Quantitive Spectroscopy and Radiative Transfer.

Bagenal, F., Mcnutt, R. L., 1989. Pluto's interaction with the solar wind. Geophysical Research Letters.

Chassefière, E., 1996. Hydrodynamic escape of hydrogen from a hot water-rich atmosphere: The case of Venus. Journal of Geophysical Research.

Gruzinov, A., 2011. The rate of thermal atmospheric escape. Arxiv.

Hunten, D. M., Watson, A. J., 1982. Stability of Pluto's atmosphere. Icarus 51, 665–667.

Jeans, J., 1925. The Dynamic Theory of Gases, 4th Edition. Cambridge, London/New York.

Johnson, R. E., 2010. Thermally driven atmospheric escape. The Astrophysical Journal.

Johnson, R. E., Combi, M. R., Fox, J. L., Ip, W. H., Leblanc, F., McGrath, M. A., Shematovich, V. I., Strobel, D. F., Waite, Jr, J. H., 2008. Exospheres and atmospheric escape. Space Science Reviews 139, 355–197.

Krasnopolsky, V. A., March 1999. Hydrodynamic flow of N2 from Pluto. JGR 104 (E3), 5955–5962.

Lammer, H., Odert, P., Leitzinger, M., Khodachenko, M. L., Panchenko, M., Kulikov, Y. N., Zang, T. L., Lichtenegger, H. I. M., Erkaev, N. V., Wuchterl, G., Micela, G., Penz, T., Biernat, H. K., Weingrill, J., Stellar, M., Ottacher, H., Hasiba, J., Hanslmeier, A., October 2009. Determining the mass loss limit for close-in exoplanets: what can we learn from transit obervations? Astronomy and Astrophysics 506 (1), 399–410.

McNutt, Jr, R. L., 1989. Models of Pluto's upper atmosphere. Geophysical Research Letters 16 (11), 1225–1228.

Murray-Clay, R. A., Chiang, E. I., Murray, N., 2009. Atmospheris escape from hot jupiters. The Astrophysical Journal.

Parker, E. N., 1964. Dynamic properties of stellar coronas and stellar winds. i. integration of the momentum equation. Astrophysics Journal 139, 72.

Strobel, D. F., 2008. N2 escape rates from Pluto's atmosphere. Icarus.

Strobel, D. F., 2009. Titan's hydrodynamically escaping atmosphere: Escape rates and the structure of the exobase region. Icaraus 202, 632–641.

Strobel, D. F., Zhu, X., 1996. On the thermal structure of Pluto's atmosphere. Icarus 120, 266–289.

Tian, F., Kasting, J. F., li Liu, H., Roble, R. G., 2008. Hydrodynamic planetary thermosphere model: 1. response of the earth's thermosphere to extreme solar euv conditions and the significance of adiabatic cooling. Journal of Geophysical Research.

Tian, F., Kasting, J. F., Solomon, S. C., 2009. Thermal escape of carbon from the early martian atmosphere. Geophysical Research Letters.

Tucker, O., Erwin, J., Deighan, J., Volkov, A., Johnson, R., 2012. Thermally driven atmospheric escape from Pluto's atmosphere: a combined fluid/kinetic model. Icarus.

Tucker, O. J., Johnson, R., June 2009. Thermally driven atmospheric escape: Monte Carlo simulations for Titan's atmosphere. Planetary and Space Science 57, 1889–1894.

Valencia, D., Ikoma, M., Guillot, T., Nettelmann, N., 2010. Composition and fate of short-period super-Earths: The case of CoRoT-7b. Astronomy and Astrophysics.

Volkov, A., Johnson, R., Tucker, O., Erwin, J., 2011. Thermally driven atmospheric escape: Transition from hydrodynamic to Jeans escape. The Astrophysical Journal Letters.

Watson, A. J., Donahue, T. M., Walker, J. C., 1981. The dynamics of a rapidly escaping atmosphere: application to the evolution of Earth and Venus. Icarus 48, 150–166.

Yelle, R. V., 2004. Aeronomy of extra-solar giant planets at small orbital distances. Icarus 170.

Zalucha, A. M., Gulbis, A. A., Zhu, X., Strobel, D. F., 2010. An analysis of Pluto occultation light curves using an atmospheric radiative-convective model. Icarus.